



DÉPARTEMENT
DE GÉOSCIENCES



PRINCETON
UNIVERSITY

INTERNSHIP REPORT - M1

Mathieu Poupon

Effect of Indian Ocean Dipole on the dynamics of oxycline and coastal anoxic events

Directed by :

Laure RESPLANDY



M1 GEOSCIENCES :
Promotion 2018

1st March 2020 – 31st July 2020

Abstract

The Indian Ocean Dipole (IOD) is an interannual variability mode of the Indian Ocean, resulting in changes in thermocline and oxycline depth. However, the interannual variability of dissolved oxygen in the Indian Ocean is unclear. The Indian Ocean hosts coastal populations that rely on fisheries resources, particularly pelagic species, as a source of food. It has been demonstrated that the distribution of these species is determined by the depth of thermocline and oxycline. Also, extreme events of coastal anoxia, causing the death of many organisms, have been recorded in the north of the basin in recent years. By compiling almost 250,000 temperature and oxygen profiles measured since 1960, this study provides a quantification of the variations in depth of the thermocline and oxycline generated by the IOD, which had been missing until then. In the eastern Arabian Sea, it is found that positive IOD phases limit the occurrence of extreme events and negative phases promote them, whereas they have the opposite effect in the eastern Bay of Bengal. This work improves the understanding of oxygen dynamics in the Indian Ocean and its OMZ, which is still poorly constrained by current models.

Keywords: *Indian Ocean Dipole, oxycline, thermocline, extreme events, oxygen, quantification*

Résumé

Le dipôle de l'océan Indien (IOD) est un mode de variabilité interannuelle de l'océan Indien, engendrant des modifications de profondeur de la thermocline et de l'oxycline. Cependant la variabilité interannuelle du dioxygène dissout dans l'océan Indien est mal connue. L'océan Indien abrite des populations côtières dont les ressources halieutiques, notamment les espèces pélagiques, font partie des sources d'alimentation. Il a été montré que la répartition de ces espèces est déterminée par la profondeur de thermocline et d'oxycline. De plus, des événements extrêmes d'anoxie côtière, causant la mort nombreux organismes, ont été recensées dans le Nord du bassin ces dernières années. En regroupant près de 250 000 profils de température et d'oxygène mesurés depuis 1960, cette étude apporte une quantification des variations de profondeur de la thermocline et de l'oxycline engendrées par l'IOD, jusqu'alors manquante. Dans l'est de la mer d'Arabie, il est mis en évidence que les phases d'IOD positives limitent l'apparition d'événements extrêmes et que les phases négatives les encouragent, alors qu'elles ont l'effet inverse dans l'est du golf du bengal. Ces travaux permettent d'améliorer la compréhension de la dynamique de l'oxygène dans l'océan Indien et son OMZ, encore mal contrainte par les modèles actuels.

Mots Clés : *Dipôle de l'Océan Indien, oxycline, thermocline, événements extrêmes, oxygène, quantification*

Contents

1	Introduction	2
2	Data and Methods	8
3	Results	11
4	Discussions	17
5	Conclusion	19
6	Acknowledgements	19

1 Introduction

Global dissolved ocean oxygen

Dissolved oxygen in the ocean has been widely observed since the second half of the 20th century. Several recent studies agree that the ocean has been losing oxygen since 1970. Based on observations, in 2017, the ocean has lost $4.18 \cdot 10^{15}$ moles of the $227.4 \cdot 10^{15}$ moles it contained in 1970, which is about 2% (Schmidtko et al. 2017; Ito et al. 2017; Helm et al. 2011). This corresponds to a rate of $96 \cdot 10^{12} \text{ mol.yr}^{-1}$ with $26 \cdot 10^{12}$ occurring between 0 and 1200m (27%). (Schmidtko et al. 2017; Oschlies et al. 2018).

These observations are consistent with models that predict a loss of 1-7% of dissolved oxygen in the ocean by 2100 (Keeling et al. 2009). The major factors controlling these losses in the context of global warming are known: decrease in solubility, reduction in circulation due to increased stratification, or decrease in the depth of the thermocline in tropical regions (Oschlies et al. 2018; Keeling et al. 2009; Long et al. 2016). However, the most recent models underestimate the rate of deoxygenation relative to observations. This is due to a lack of understanding in the modelling of biogeochemical processes and circulation (Oschlies et al. 2018; Stocker et al. 2013). Also, interannual variability is underestimated by the models when compared to the observations. (Long et al. 2016; Oschlies et al. 2018).

Oxygen Minimum Zones (OMZs)

The distribution of dissolved oxygen is heterogeneous in the oceans on a global scale. Minimum Oxygen Zones (OMZs), also known as 'shadow zones', are observed where oxygen concentrations fall below $60 \mu\text{mol.L}^{-1}$, usually between 200 and 1000 m. It can be defined as the hypoxic threshold. According to World Ocean Atlas (WOA) data, their volume is estimated at $15 \cdot 10^{15} \text{ km}^3$ (Levitus

et al. 2010). Observations show that these areas are also expanding, about 5% in total since 1970 (Schmidtko et al. 2017), with an oxygen loss rate around $0.15 \mu\text{mol}.kg^{-1}.\text{yr}^{-1}$ over the last 50 years, but the uncertainties are large (Levin 2018; Stramma et al. 2008). Because of the lack of understanding of the processes that drive the dynamics of oxygen, models do not predict robust trends in OMZ dynamics (Keeling et al. 2009; Fu et al. 2018; Oschlies et al. 2018)

The largest OMZs are located in the Pacific, and are associated with significant upwelling initiated by westerly currents. In these areas the measured oxygen losses are higher than the global average (-4%). The main cause is the high consumption of O_2 by remineralisation (Keeling et al. 2009). These areas are very productive because of the important upwellings bringing nutrients to the surface. The third largest OMZ in the world is located in the Northern Indian Ocean (Fig 1, b). It is different from the others because it is located in two semi-enclosed basins: the Arabian Sea and the Bay of Bengal. Also, it hosts about 21% of the world's hypoxic waters (Acharya and Panigrahi 2016). The coasts of these basins host the largest hypoxic ($< 60 \mu\text{mol}.L^{-1}$) coastal system in the world (Fig 1, a) controlled by a seasonal cycle, but which also seems to be subject to interannual variability (Naqvi et al. 2009).

OMZs and oxygen impacts on ecosystems and biogeochemical cycles

Understanding the dynamics of oxygen in this region, as in the rest of the Indian Ocean, is important because it is involved in modifying biogeochemical cycles, and also in the structuring of the ecosystems they host. In suboxic waters ($1 - 5 \mu\text{mol}.L^{-1}$), denitrification is observed (Dalsgaard et al. 2014), because of the low O_2 concentration causes some bacteria to use nitrate as an electron acceptor instead of oxygen to oxidize organic matter. This process produces N_2O , which is a greenhouse gas, and N_2 as a gas that escapes into the atmosphere, reducing the amount of dissolved nitrogen in the ocean. When waters become anoxic ($< 0.1 \mu\text{mol}.L^{-1}$), especially near the coast, sulphate may be used as an electron acceptor and reduced to S_2H . In this case, the waters are euxinic (Naqvi et al. 2006; Thamdrup 2012).

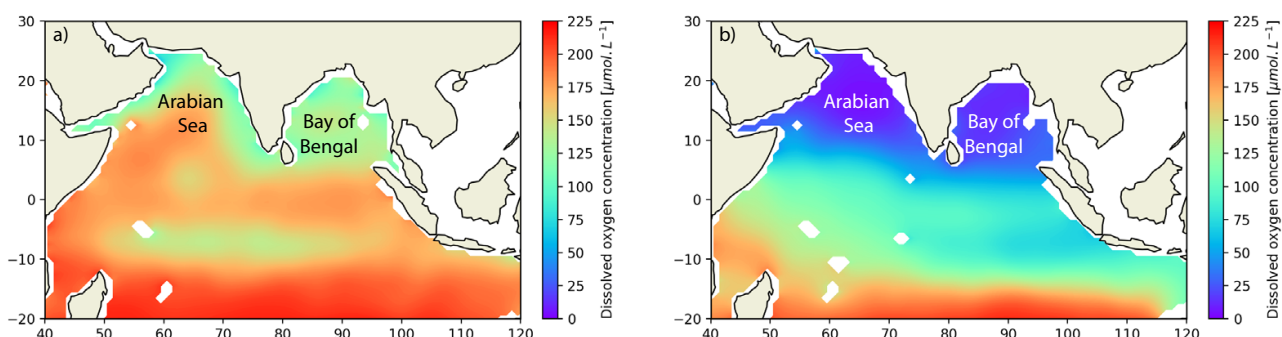


Figure 1 – Observed climatological dissolved oxygen concentration at 50m (a) and 300m (b) in the Indian Ocean based on the World Ocean Atlas 2018.

The depth of the oxycline determines the structure of ecosystems, for example the location of marlins, which do not occupy waters below $155 \mu\text{mol.L}^{-1}$, and tuna (Stramma et al. 2012; Ingham et al. 1977). In the western Indian Ocean, off the coast of Comoros, there is an important correlation between oxycline depth and the distribution of tuna (Cayré and Marsac 1993). The expansion of the OMZ and the rise of the thermocline lead to a compression of the niches occupied by these species (Stramma et al. 2012). Indeed, waters with low oxygen levels ($< 60 \mu\text{mol.L}^{-1}$) lead to deficiencies in many species such as sub-optimal reproduction rates and death (Vaquer-Sunyer and Duarte 2008). For example, about 50 fish have shown deficiencies for O_2 thresholds below $133 \mu\text{mol.L}^{-1}$ (Sokolova 2013; Ekau et al. 2010). This compression of ecological niches, associated with overfishing, increases the vulnerability of marlin and tuna populations. The expansion of OMZs is also associated with a 10-50% drop in pelagic biodiversity (Stramma et al. 2012). Understanding the evolution of the oxycline and thermocline in the Indian Ocean is therefore important for locating fishery resources and anticipating their evolution.

The hypoxic coastal waters, also known as 'dead zones', whose numbers have increased exponentially since 1960, harbour unviable conditions for organisms such as fish (Diaz and Rosenberg 2008). These sites are mostly located along the European and American coasts. In the Indian Ocean, they are located along the west coast of India and east of the Bay of Bengal (Breitburg et al. 2018). The number of these sites seems to be underestimated (Vaquer-Sunyer and Duarte 2008). In some years, oxygen concentrations can become anoxic (Parvathi et al. 2017). These are extreme events which can cause widespread death in fish populations, weakening the fishing and food supply of coastal populations. These events are also involved in the extinction of coral reefs (Altieri et al. 2017). To assess the risks and predict these events, it is essential to understand what factors control oxygen in the northern Indian Ocean.

Factors controlling the dynamics of the Northern Indian Ocean OMZ

On a global scale, oxygen is controlled by a balance between solubility, mixing/circulation and biological consumption (Oschlies et al. 2018). However, the Indian Ocean OMZ is atypical because this ocean is closed to the North. For this reason, ventilation of subsurface waters is slow. O_2 input comes mainly from waters formed in the Southern Ocean. The main source of oxygen is remineralization in the subsurface waters, as surface productivity is high. However, the physical dynamics of the Indian Ocean has an important role in controlling the dynamics of the OMZ as well. Southern waters are advected along the Somali Current, propagate into the OMZ and counterbalance biological consumption (Resplandy et al. 2012). Seasonality of the OMZ is mainly driven by Ekman pumping generated by monsoon winds on a seasonal scale. On the annual scale, mesoscale structures maintain the oxygen concentration equilibrium. Coastal Kelvin and Rossby wave propagation also modify coastal oxygen concentrations. There is a need to improve our understanding of the balance between the physical and biological processes that control O_2 and OMZ (Resplandy et al. 2012).

Physical dynamics of the Indian Ocean

- Seasonal Variability: Monsoon circulation

The most significant seasonal variability is located in the northern Indian Ocean. It corresponds to the monsoon phenomenon, which is divided into four phases: summer (southwest) and winter (northeast) monsoons, and inter-monsoons between monsoons. Seasonal wind variations cause currents to reverse (Somali Current (SC), Southwest /Northeast Monsoon Current (SMC/NMC)). During the summer monsoon, a south-westerly wind (Findlater jet) blows along the Arabian Peninsula towards the centre of convection located over India (Fig 2, e). The Wyrtki Jet blows from west to east across the equator. In winter, the shift of the convection centre in the South Arabian Sea reverses the Findlater jet and slows down the Wyrtki jets.

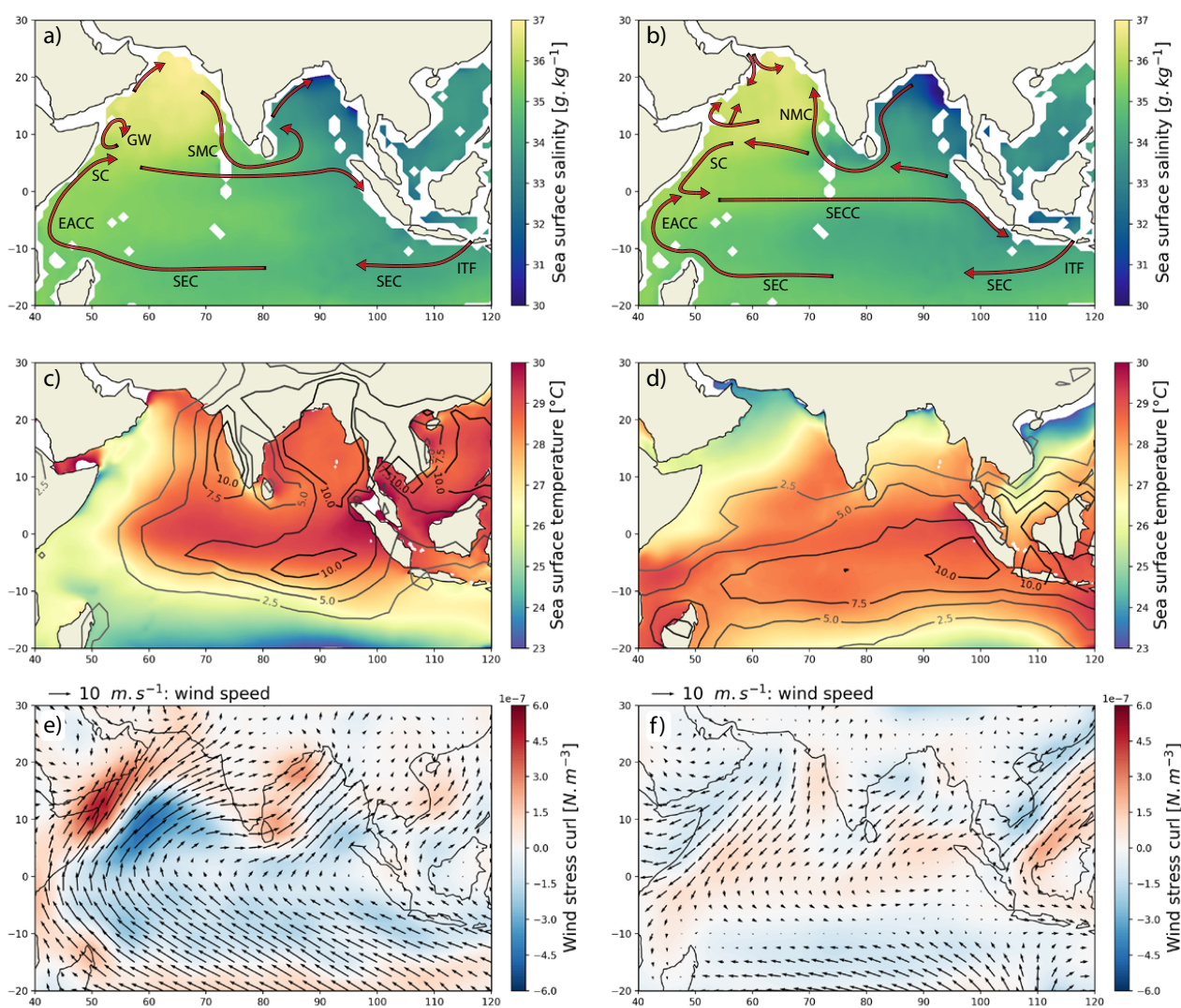


Figure 2 – Summer monsoon climatology (June, July, August) of: sea surface salinity (colour) and main surface currents (arrows, from Schott et al. 2009) (a), sea surface temperature (colour) and precipitation rate [$\text{mm} \cdot \text{day}^{-1}$] (contour lines) (c), horizontal wind speed (arrows) and wind stress curl (colour) (e). Same for the winter monsoon (December, January, February): (b,d,f).

In the upper ocean, the SEC (between 20-10°S) carries the waters, flowing out of the Pacific through the Indonesian Throughflow (ITF), from east to west to the African coast. Some of this

water rises along the Somali coast during the summer monsoon and supplies the Northward Somalian Current (Fig 2, a). Some of these waters, pushed by the wyrkti jet, flow from west to east through the South Equatorial Countercurrent (SECC). Others spread as far as the North Arabian Sea, notably via gyres (the largest of which is the Great Whirl (GW)) and then flow down along the coast of India via the SMC and supply the Bay of Bengal (Fig 2, a). During the inter-monsoon period, the Findlater jet reverses. During the winter monsoon, because of the wind inversion, the currents are reversed in the northern Indian Ocean. The SMC flows from the Bay of Bengal to the North Arabian Sea along the Indian coast and the Somalian Current flows southward (Fig 2, b).

At intermediate depths, Indian Central Water is supplied by oxygenated water formed in Antarctica. Indian Central Water (ICW) provides oxygen to the OMZs in the Arabian Sea and Bay of Bengal, but ventilation is poor due to the closure of the basin to the north.

Precipitation is localized in the Northeast Indian Ocean during the summer and in the South during the winter, following the regions of high sea surface temperature (SST). There is a significant overlap of precipitation and SST patterns, indicating a strong coupling in these two fields. Winter cooling in the North Arabian Sea is important because of the latent heat loss caused by dry, cold winds. In the western Arabian Sea, there is strong cooling during the summer due to upwelling along the coasts of Somalia and Oman caused by strong southwest winds from the Findlater jet (Fig 2, c and d).

On the surface, the Arabian Sea is very salty because it receives water from two evaporation basins: the Red Sea (Red Sea Water: 36.5 g.kg^{-1}) and the Persian Gulf (Persian Gulf Water: 37 g.kg^{-1}) (Acharya and Panigrahi 2016). While the Bay of Bengal receives water from rivers with low salinity ($< 27 \text{ g.kg}^{-1}$, Jana et al. 2015), as well as precipitation (Fig 2, c and d). This salinity differential between surface and intermediate waters makes the Bay of Bengal highly stratified. In contrast the Arabian Sea is an evaporation basin subject to vertical movements.

During the summer monsoon, significant upwelling develops in the eastern Arabian Sea, due to coastal effects and positive Ekman pumping (Fig 2, e), and also along Java and Sumatra. Ekman pumping is also observed in the western Bay of Bengal; however, the high stratification limits upwelling. In winter, upwelling develops in the Arabian Sea along the Indian coast (Fig 2, f). These upwellings bring nutrient-rich waters to the surface and create areas of high phytoplankton productivity. Remineralization of this production consumes oxygen and maintains OMZs and the coastal hypoxic system.

- Interannual Variability: Indian Ocean Dipole (IOD)

Several modes of interannual variability are superimposed in the Indian Ocean: El Niño-Southern Oscillation (ENSO) and IOD. There is a global warming of the basin during El Niño years, but in some years there is a positive temperature anomaly only to the west of the basin, and a negative anomaly

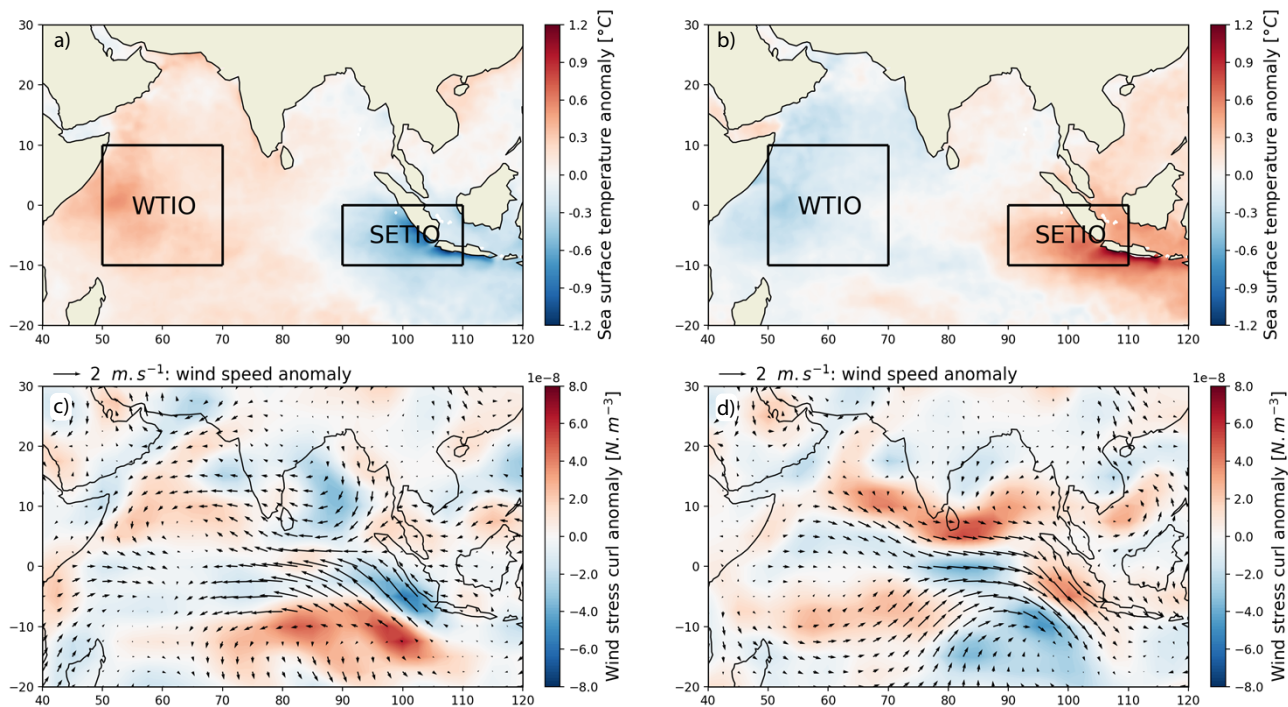


Figure 3 – IOD positive phase climatology: of the sea surface temperature anomaly (a), the wind speed anomaly (c, arrows) and the wind stress curl anomaly (c, colour). The same for the negative phase: (b,d). The sea surface temperature anomaly in the WTIO and SETIO boxes are used to calculate the Dipole Mode Index (DMI). The positive (negative) phase corresponds to a DMI higher (lower) than $+/-$ a standard deviation.

to the east (Fig 3, a), as well as a shift in cloud formation and zonal wind anomalies. These anomalies cannot be explained by ENSO, especially in 1997 (Schott and McCreary Jr 2001).

At the end of the 20th century, the covariance of these different anomalies is demonstrated using 40-year time series and identifies the IOD (Saji et al. 1999). An index is defined and used to characterize the phase of the dipole: The Dipole Mode Index (DMI). This index corresponds to the temperature anomaly difference between the Western and Southeastern Tropical Indian Ocean (WTIO and SETIO) boxes. Positive (negative) phases are defined by a large positive (negative) DMI. During a positive phase, the temperature anomaly is positive in the west and negative in the east (Fig 3, a). Westerly winds weaken at the equator, allowing the thermocline and cold water to rise along Sumatra (Fig 3, c). An increase in rainfall is also observed over eastern Africa and a decrease over northern Australia. During negative phases it is the opposite (Fig 3, b and d). This anomaly develops in June and reaches its maximum in October. The ascent of the thermocline in summer along Sumatra is a favourable factor for the development of Bjerknes feedback (Schott et al. 2009).

During the different phases of the IOD, Rossby and Kelvin waves propagate along the equatorial band, the coasts of Sumatra and the northern ocean. The propagation of these waves contributes to the change in the depth of the thermocline (Yuan and Liu 2009). In the Indian Ocean, thermocline and oxycline variations are linked. To understand the basin-wide variations in oxycline depth, the effect of IOD-related waves must therefore be studied. Some models also assume that these waves

may promote or limit extreme events near the coast, especially through the propagation of coastal Kelvin waves (Parvathi et al. 2017)

Objectives

Gaps in understanding the effects of interannual variability in the Indian Ocean on oxygen dynamics are significant. In particular, there is a significant lack of data and quantification of variations. The first objective here is to quantify oxycline and thermocline variations related to the IOD. These variations are important for locating fishery resources. Then, in order to improve risk evaluation related to extreme coastal events, the second objective is to quantify the effect of the dipole on these events.

2 Data and Methods

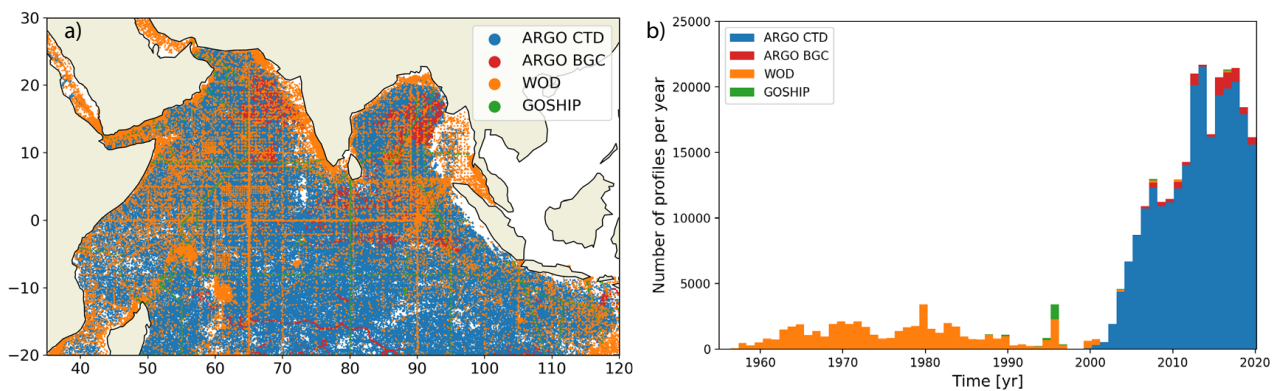


Figure 4 – Spatial (a) and temporal (b, number of profiles measured per year) distribution of profiles. The colour corresponds to the profile database: World Ocean database (orange), GO-SHIP database (green), Argo CTD floats (blue) and BGC floats (red).

Temperature and oxygen profiles

In this study, 248 975 profiles, distributed over 62 years, are used. They are the result of the merging of several databases: the World Ocean Database 2018 (WOD), GO-SHIP cruises and the ARGO database (CTD and BGC). In terms of spatial coverage, for the majority of the basin, ARGO CTD profiles dominate the sampling, while in the coastal domain WOD profiles dominate. (Fig 4, a). In terms of temporal coverage, the WOD contains almost all the profiles measured in the 20th Century. Then in the 21st Century, the deployment of the ARGO float system resulted in a more than 10-times increase in the number of profiles measured in the basin each year (Fig 4, b). The ARGO BGC, WOD and GOSHIP floats contain temperature and oxygen profiles. However, the ARGO CTD floats do not measure oxygen. In some areas, especially the southern hemisphere of the basin, very little, if any, oxygen is sampled (Fig 4, a). Oxygen and temperature profiles from the WOD and ARGO database are filtered based on their quality using only the highest quality flags. All profiles

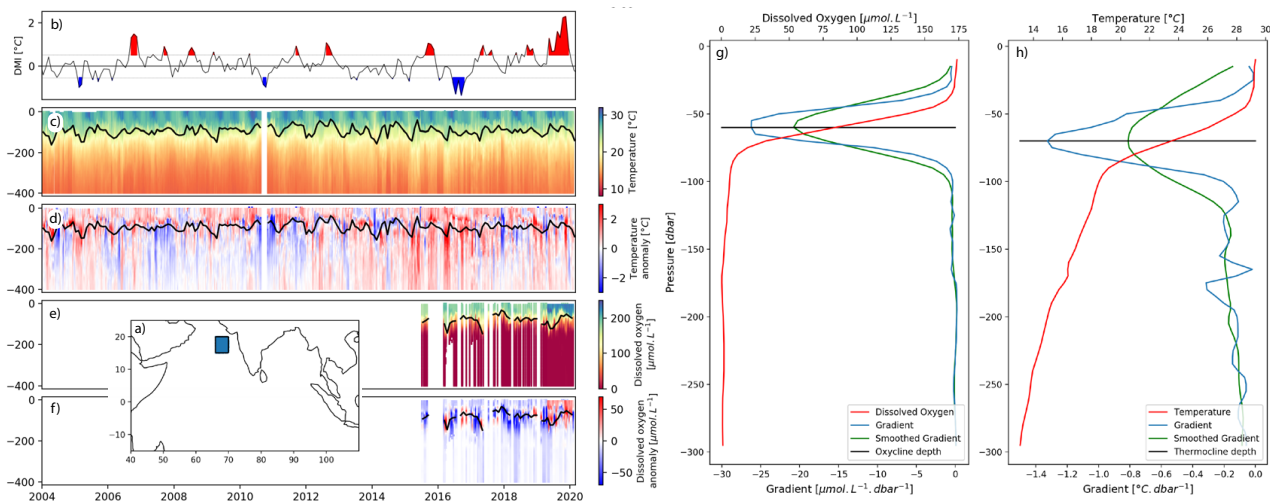


Figure 5 – Time series of the DMI (b), positive (negative) phases are red (blue). Temperature (c) and oxygen (e) profiles measured in the box (12–17°N, 66–70°E) (a) between 2004 and 2020. Or calculated profiles: anomaly of temperature (c) and oxygen (e). The black line corresponds to the monthly mean thermocline (c, d) and monthly mean oxycline (e, f). Example of oxycline calculation (g) (thermocline, h). The red line is the oxygen profile (temperature), the blue line is the raw gradient and the green line is the smoothed gradient. The black line corresponds to the calculated oxycline depth (thermocline).

are interpolated between 0 and 800m with a 5m step. In addition to these raw data, the World Ocean Atlas 2018 (WOD) is used as a reference for the monthly mean ocean state.

Profile analysis: oxycline, thermocline and anomaly

For each temperature (Fig 5, c) and oxygen profile (Fig 5, e), a characteristic depth (thermocline or oxycline) is calculated. Compared to Parvathi et al. (2017), or Resplandy et al. (2012), the oxycline and thermocline are not determined by fixed thresholds but by a gradient extremum. The gradient is calculated over the entire profile and then smoothed by applying a running average (Fig 5, g and h). This filters out local gradient irregularities and defines a characteristic depth representative of the profile. The advantage of using the gradient extremum with respect to a threshold is that it does not depend on variations in average temperature and oxygen in the basin.

For each profile, the thermocline or oxycline anomaly (Fig 5, d and f) is calculated as the difference between the characteristic depth of the profile and that of the geographically closest WOA profile of the same month. The same goes for temperature and oxygen anomaly profiles. An example of all these values is illustrated (Fig 5).

IOD and variability index

The index characterizing the phases of the Indian Ocean Dipole: Dipole Mode Index, is defined as the difference between 2 indices: WTIO and SETIO. Each index corresponds to the mean temperature anomaly in the corresponding box (WTIO: 10°S - 10°N, 50 - 70°E | SETIO: 10°S - 0°N, 90-100°E | see

Fig 3: a and b):

$$DMI = WTIO - SETIO$$

To obtain a series of DMIs over the entire time series (Fig 6) covered by the set of profiles (Fig 4, b), two different databases with monthly resolution are used. The first (green line), covering the period from 1958 to 1999, is the one defined and used by Saji et al. (1999). The second, covering 1981 to 2020 (blue line), comes from NOAA: <https://stateoftheocean.osmc.noaa.gov/sur/ind/dmi.php> and is still being updated. The first has been weighted to have the same standard deviation as the second during the common measurement period (1981-1999).

A positive (negative) IOD phase is defined as a period when the DMI is higher (lower) than plus (minus) a standard deviation. These periods are filled in red (blue), (Fig 6).

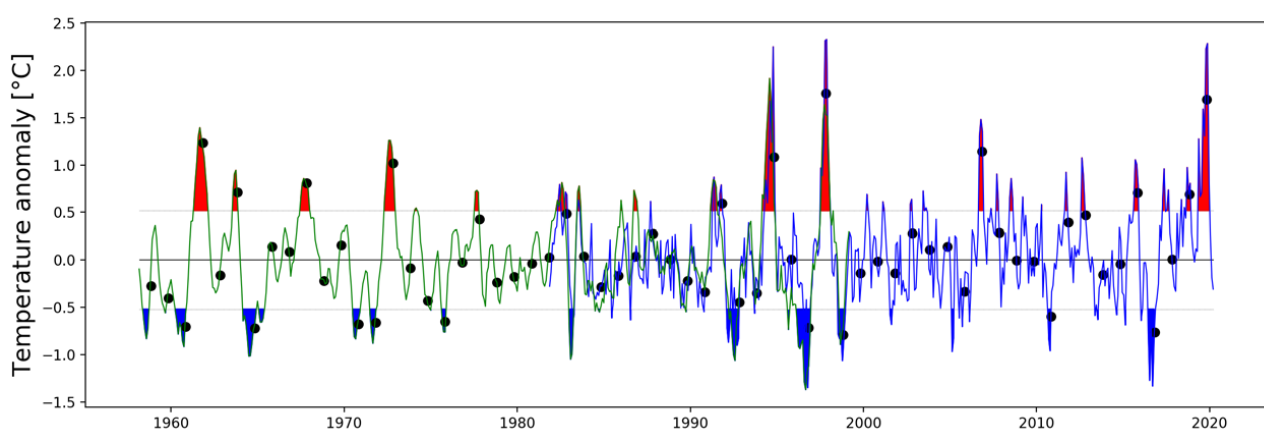


Figure 6 – DMI time series from 1958 to 2020. The green line corresponds to the series of (Saji et al. 1999) from 1958 to 1999 and the blue line to the NOAA series from 1981 to 2020. The black dots correspond to the average DMI between October and November. Positive (negative) IOD phases are red (blue).

As IOD is a process involving wave propagation, the effects of these phases can be shifted in time depending on the geographical location of the profiles. For each profile, an average index (black dots, Fig 6), representative of the IOD, is defined to take into account lag related to wave propagation. It corresponds to the average of the DMI peak in October and November (months of maximum IOD anomaly). This index is associated to the profiles of the same year from July to December and to those of the following year from January to June.

Satellite data

All data fields have a monthly resolution. The sea surface temperature (SST) fields are from NOAA (www.ncdc.noaa.gov/oisst). They are built from satellites, argo floats, boats and buoys data. They extend from 1981 to 2018 with a spatial resolution of 0.125° . Sea surface salinity (SSS) data spanning from 2011 to 2019 are from NASA's Aquarius program. The spatial resolution is 1° .

The zonal and meridional surface winds are derived from NCEP reanalyses from 1948 to 2020 at 0.75° resolution. They are used to calculate the wind stress curl according to the following formula:

$$\tau = \rho_{air} \cdot c_d \cdot U_h^2$$

$$Curl(\tau) = \frac{\partial \tau_y}{\partial X} - \frac{\partial \tau_x}{Y}$$

With: U_h the horizontal wind velocity, $\rho_{air} = 1.225 \text{ kg.m}^{-3}$ the air density and $c_d = 0.0015$ the wind drag coefficient. The interannual anomaly is the difference between a measurement and its mean for the same month over the entire time series.

Sea surface height (SSH) data extends from 1992 to 2020 with a resolution of 1°. They are produced by combining satellite observations (www.aviso.altimetry.fr). Finally the precipitation data extend from 1979 to 2019 with a resolution of 2.5°, and are the result of NCEP/NCAR reanalysis.

Selection of Study Area Boundaries

The study focuses on oxycline and thermocline variations, which are related. SSH is a good proxy for these variations. The study area is defined by looking at the areas of greatest SSH variation, calculating its interannual standard deviation (standard deviation of all SSH measurements minus their monthly mean, Fig 7). The main patterns of variability are above 20°S. This value therefore determines the southern limit of the study. To the east, the limit is 120°E.

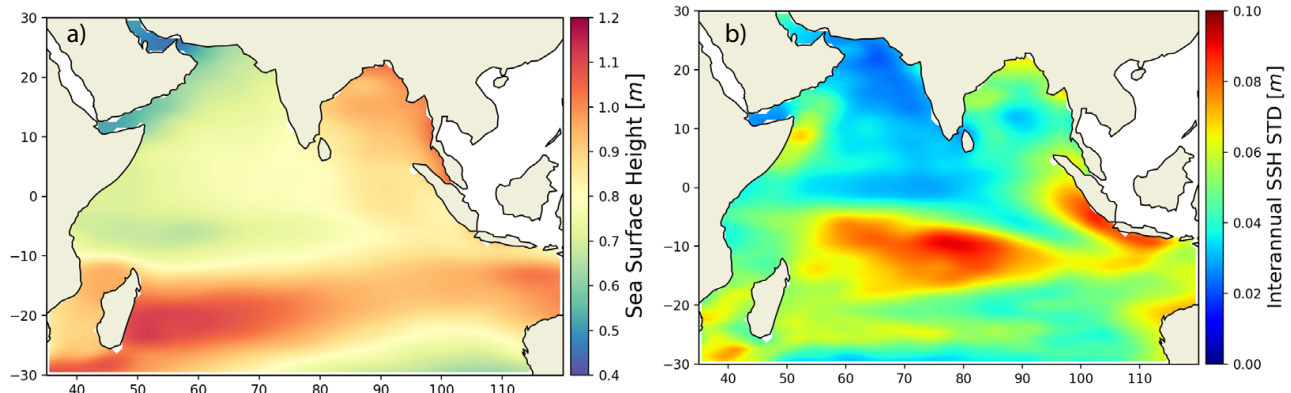


Figure 7 – Sea surface height climatology (a) and interannual standard deviation (b)

3 Results

Thermocline and oxycline variability during IOD phases

- Relationship between thermocline and oxycline variations across the Indian Ocean

Figure 8 shows the observed climatology of the thermocline depth and oxycline obtained by gridding the profiles on a regular $1^\circ \times 1^\circ$ grid, then smoothing with a Gaussian filter. The structures already identified in the bibliography such as the thermocline ridge (shallow thermocline between 15-5°S and 45-90°E) or the Great Whirl are highlighted by the depth of the thermocline (a). The signature of these structures is reflected in the distribution of the oxycline (b). The major differences between these two maps are a shallower oxycline than the thermocline along Java and Sumatra, the Bay of Bengal and the west coast of India. This difference varies from about 10 to 30 dbar. This oxycline and thermocline climatology corresponds to the state of the Indian Ocean in the neutral phase of IOD.

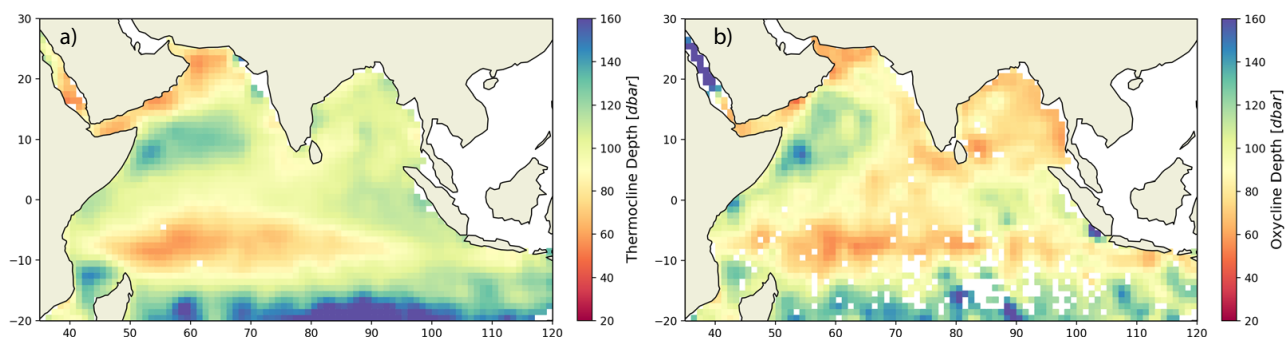


Figure 8 – Climatology of thermocline depth (a) and oxycline depth (b) from raw profiles. The maps are smoothed with a Gaussian filter to remove noise

To understand how these characteristic depths vary from one another, Figure 9 shows the distribution of the linear regression slope and correlation of oxycline versus thermocline on a seasonal (a), and interannual (b) scale (regression of oxycline anomaly versus thermocline anomaly). In a large band south of the basin ($20\text{-}10^\circ\text{S}$, $65\text{-}105^\circ\text{E}$), the lack of O_2 data results in many unsampled areas and a low correlation (< 0.3). In the rest of the basin, as seen in Fig 9 (a), the correlation is above 0.5 on a seasonal scale. It rises above 0.7 in some areas, especially around the centre of the thermocline ridge, along Sumatra and the coasts of India. In these areas, a variation of 1 dbar in the thermocline generates about a 1 dbar variation in the oxycline, in contrast to the rest of the basin where this variation is halved, i.e. a variation of 1 dbar generates a variation of about 0.5 dbar in the oxycline depth. At the interannual scale (as seen in Fig 9, b) the correlation is smaller, but still not negligible (higher than 0.5 in the highest correlated areas), and we find in these areas a variation of 0.7 dbar of oxycline anomaly for a change of 1 dbar of the thermocline. Thermocline variations are therefore a good proxy for oxycline variations on both seasonal and interannual scales. This confirms the importance of ocean physics on the control of O_2 in the Indian Ocean.

- IOD phases and magnitude of thermocline and oxycline variation

The thermocline varies according to the IOD phases. Figure 10 quantifies this variation by representing the distribution of the linear regression slope of the thermocline as a function of the mean of the DMI peak in October and November. There is very little correlation between this variation

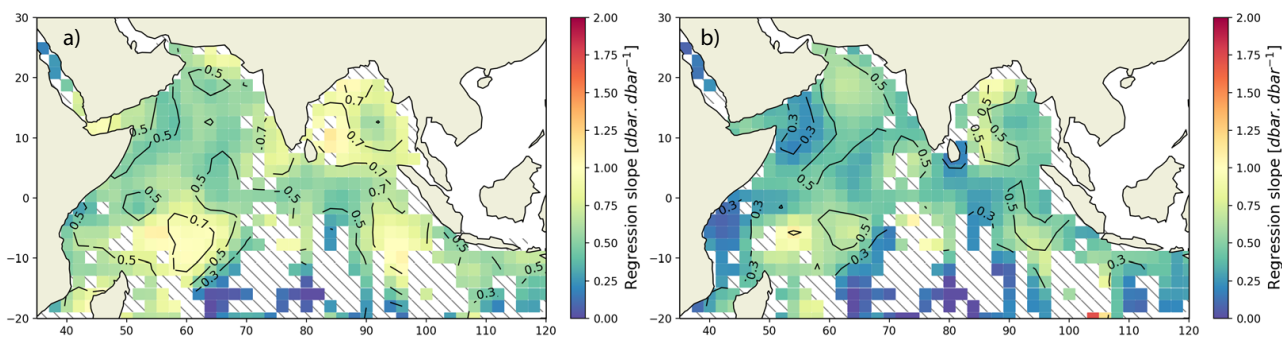


Figure 9 – Seasonal (a) and interannual (b) correlation (contour) and regression slope (color) between thermocline and oxycline depths.

in the Arabian Sea and the western Indian Ocean. At the eastern limit of the thermocline ridge, the regression coefficient is positive, so the thermocline deepens (rises) on a positive (negative) event. This variation is about 20 to 30 dbar per degree of DMI, and the DMI can rise by up to 2°C . Along the east coast of the basin, the regression coefficient is negative. The thermocline rises (deepens) during positive (negative) IOD phases, from 15 to 25 dbar per degree of DMI. This signal propagates to the middle of the basin at the equator, and along the Bay of Bengal coast. Quantification of these thermocline variations related to IOD phases are important for the location of fishery resources, as are oxycline variations.

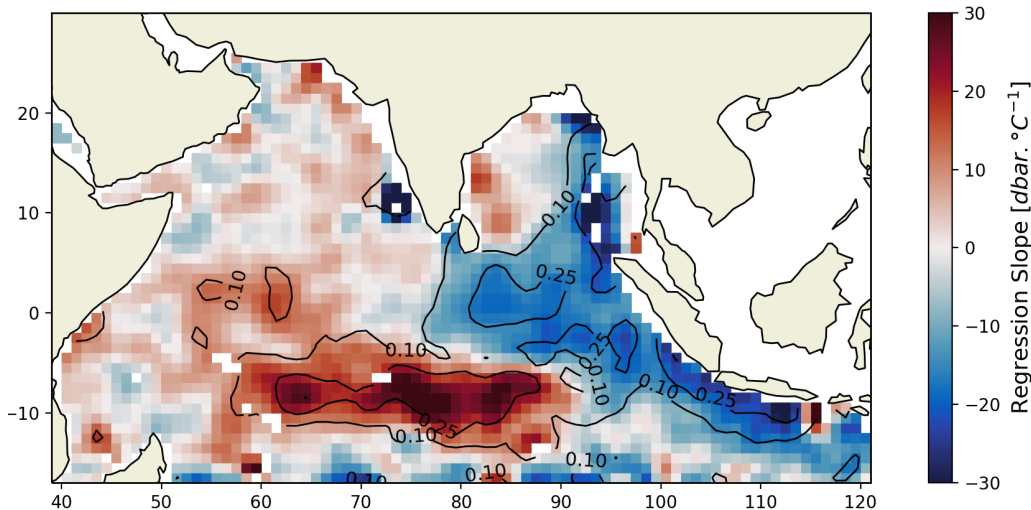


Figure 10 – Correlation (contour) and linear regression slope (color) of the thermocline depth relative to the mean DMI between October and November.

The oxycline variations as a function of IOD phase are reconstructed by multiplying the interannual oxycline variations as a function of thermocline interannual variations (Fig 9) by the thermocline variations as a function of DMI (Fig 10). Figure 11 shows the climatology of the thermocline and the oxycline reconstructed from the thermocline during the positive and negative IOD phases (average of the DMI peak between October and November higher/lower than +/- one standard deviation). The same trends as in Figure 10 are observed for the thermocline (Fig 11, a,c). At a positive IOD, a positive anomaly (deepening) of 10 to 20 dbar is observed between $15\text{--}5^{\circ}\text{S}$ and $60\text{--}90^{\circ}\text{E}$ (Fig

11, a). This signal appears to propagate in the South Arabian Sea with an intensity slightly below 10 dbar. A negative signal propagates along the western coasts of the basin and up to 80°E at the equator, a rise in the order of 10 to 20 dbar. During a negative phase (Fig 11, c), the effects seem more localised. Between 15-5°S and 80-90°E, an upwelling of 30 to 40 dbar is observed. For the rest of the basin, the amplitude of the variations is less important than during the positive phases. This can be explained by the fact that the negative phases have a lower amplitude than the positive phases (Fig 6). Also, the thermocline ridge is characterized by a shallow depth (Fig 8), so it may be more difficult for it to rise higher, as the stratification is stronger at the surface.

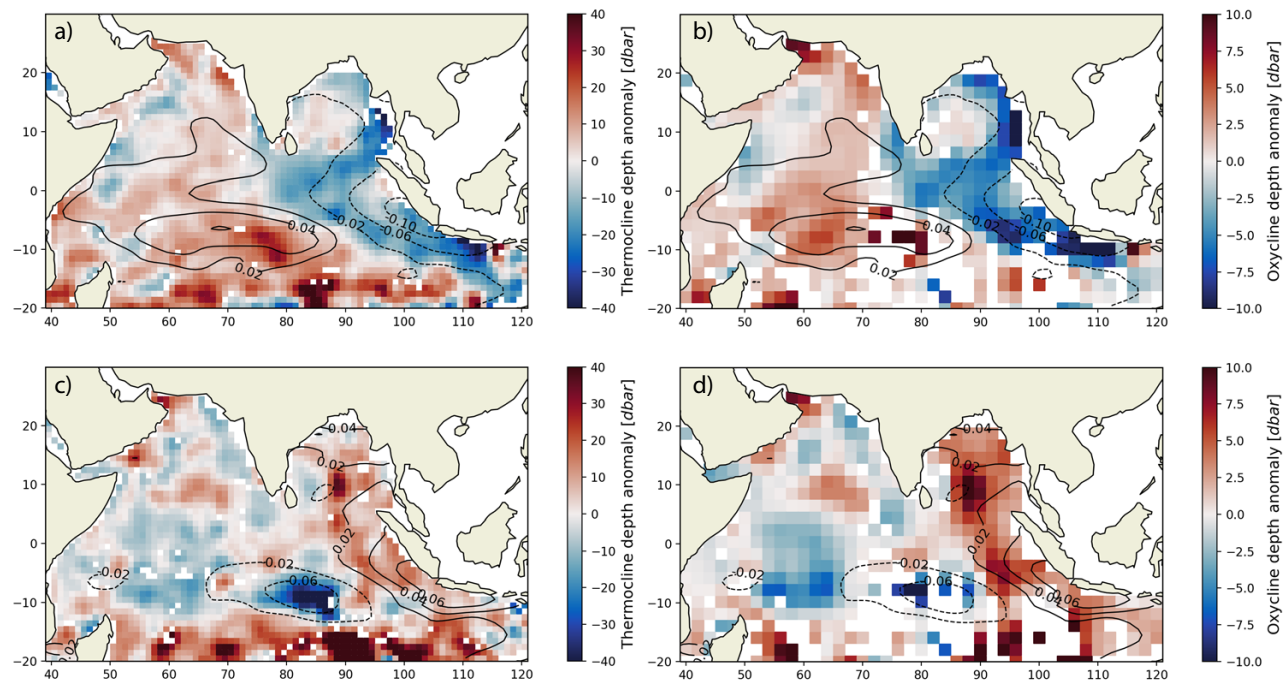


Figure 11 – Positive IOD phase climatology of the sea level anomaly [m] (contour, a and b), the thermocline depth anomaly (color, a) and the thermocline-derived oxycline depth anomaly (color, b). Same for the negative IOD phase (c, d). Solid lines indicate positive SLA and dashed lines indicate negative SLA.

Composites of oxycline anomaly reconstructed from the thermocline anomaly (Fig 11, b,d) are of lower amplitude than those of the thermocline anomaly (as shown in Figure ,9,b used to reconstruct oxycline variations). A rise (deepening) of the oxycline is estimated at 5 dbar between 15-5°S and 60-90°E, during a positive (negative, d) IOD phase. In a positive IOD (b), oxycline appears to rise by 10 dbar along the west coast and in the western Bay of Bengal, which is relatively important because in this area the depth of oxycline is 60 dbar on average. The same is true for the negative phase (d), in these same areas, where the sinking of the thermocline is estimated at 5-10 dbar. Moreover, the two phases seem to have opposite effects on the west coast of India. The positive phase seems to sink the thermocline by about 10 dbar, while the negative phase lifts it by the same order of magnitude.

In most of the basin, the oxygen concentration in the first 50 metres (Fig 1, a) is sufficient for the development of pelagic species. But in the thermocline ridge, and the coasts of the Arabian Sea

and Bay of Bengal, average concentrations reach the limit of the disturbance thresholds for these species. Quantification of these oxycline and thermocline variations is thus important in locating these ecosystems. In addition, these anomaly patterns are superimposed on the sea level anomaly (SLA) composites (Fig 11). Therefore, each SLA value can be associated with a thermocline and oxycline anomaly value in each region. Since SLA is measurable by satellite altimetry, forecasting the location of fishery resources in real time can be carried out.

Effect of IOD Phases on coastal extreme events

- Period favourable for extreme events preconditioning

The Indian Ocean dipole generates the propagation of many waves. It is possible that several waves of different polarities pass at the same place during the same IOD event, especially in the coastal domain. To understand the precise effect of the dipole on extreme coastal events, it is therefore important to know the period when seasonal conditions precondition these events. Extreme events are characterized by a drop in oxygen concentration and a rise of oxycline at the surface. It is assumed that the period preconditioning an extreme event is the month of the year when the oxycline is shallowest at a given point. In this section, attention is focused only on profiles measured less than 300 km from the coast.

In areas where extreme events have been detected, i.e. the west coast of India and the eastern Bay of Bengal, the oxygen concentrations in the minimum oxycline months are different (Fig 12). The mean concentration in the water column falls below $100 \mu\text{mol.L}^{-1}$ between 10 and 50 m along the Indian coast, while in this depth range it remains above $150 \mu\text{mol.L}^{-1}$ in the eastern Bay of Bengal (Fig 12, a). Between 50 and 200m, oxygen concentration falls below $100 \mu\text{mol.L}^{-1}$ and approaches hypoxic concentrations ($60 \mu\text{mol.L}^{-1}$) in the eastern Bay of Bengal (Fig 12, b). To study the effect of IOD phases on oxygen distribution, the mean concentration between 0 and 50m will be studied for the west coast of India and between 0 and 200m in the Bay of Bengal.

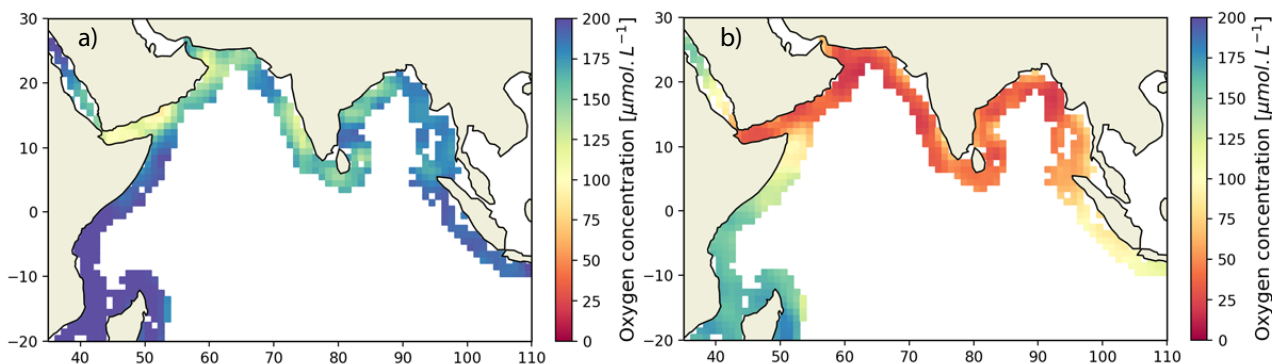


Figure 12 – Average oxygen concentration between 10 and 50m (a), 50 and 200m (b) during the month of minimum oxycline depth, for coastal profiles (300 km from the coast). A Gaussian filter is applied to remove noise.

- Effect of IOD phases on extreme events

The months of minimum oxycline are different in the two zones. Along the west coast of India, this period corresponds to the months of September and October, whereas it corresponds to January and February in the Bay of Bengal (Fig 13,a).

To analyse the effect of the IOD phases, an IOD phase is associated to each profile measured in these two zones (negative, positive or neutral), according to the average peak of IOD between October and September associated with each profile (higher than one standard deviation: positive, lower than minus one standard deviation: negative, otherwise neutral). The distribution of mean O₂ concentration in the water column under study (0-50 m , 0-200m) is then examined as a function of phase and study area. In Figure 13, the raw normalized distribution of mean O_2 concentrations is represented by the histograms (One bar covers $10 \mu\text{mol.L}^{-1}$, ranging from 0 to $230 \mu\text{mol.L}^{-1}$), while the lines represent a Gaussian fit of the histograms.

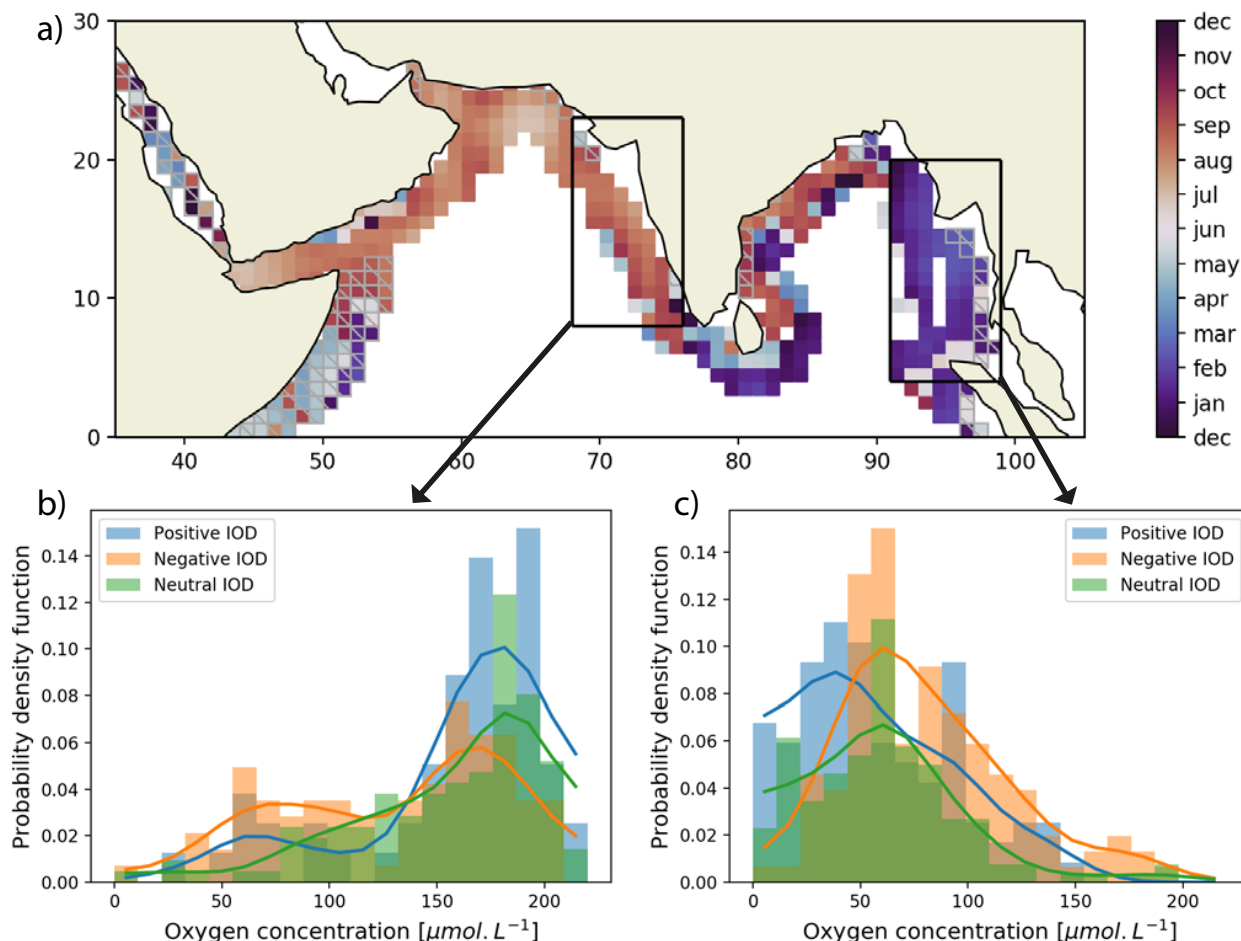


Figure 13 – Months of minimum oxycline depth, a Gaussian filter is applied to remove noise. Grey hatches corresponds to areas where the mean oxygen concentration between 0 and 200m is higher than $100 \mu\text{mol.L}^{-1}$. (a). Probability distribution function of the mean oxygen concentration during the minimum oxycline month, between 0 and 50m in the western box (b), between 0 and 200m in the eastern box (c), depending on the IOD phase: negative (orange), neutral (green) and positive (blue). The bar plots correspond to the actual data and the lines to a Gaussian fit.

Along the Indian coast, waters rich in O_2 ($> 150 \mu\text{mol.L}^{-1}$) are more observed in positive phases than in neutral phases, with a frequency peak at $180 \mu\text{mol.L}^{-1}$. They are less observed during negative phases than during neutral phases, and therefore also less than during positive phases (half). On the other hand, waters low in O_2 ($< 100 \mu\text{mol.L}^{-1}$) are twice as much observed during the negative phases of the IOD as during the positive or neutral phases. The negative phases of the dipole tend to increase the probability of hypoxic events near the coasts. On the other hand, positive phases tend to increase the O_2 concentration in the first fifty meters of the water column and hence limit the probability of hypoxic events.

In the eastern Bay of Bengal, the mean O_2 concentration in the first 200 metres is mostly around $60 \mu\text{mol.L}^{-1}$, but ranges largely between 0 and $100 \mu\text{mol.L}^{-1}$. During positive phases, there is half as much water below $30 \mu\text{mol.L}^{-1}$ as during neutral phases and an increase in the observation of O_2 -rich water ($> 100 \mu\text{mol.L}^{-1}$). In the positive phases, it is the opposite, we observe an increase in hypoxic water, twice as much as in the neutral phases and four times as much as in the negative phases. In this area, positive IOD phases seem to increase the probability of hypoxic events, while negative phases seem to limit them. This is in contrast to what we see along the Indian coast.

4 Discussions

Wave propagation during IOD phases

The effects of IOD phases on oxygen concentrations in the water column can be explained by wave propagation caused by jet anomalies around the equator. The effect of the propagation of these waves on the SLA has been documented by Suresh et al. (2018), but the SLA, the thermocline depth and the oxycline depth are related. During a positive phase, the jet anomaly generates upwelling Kelvin waves propagating eastward and downwelling Rossby propagating westward at the equator (Fig 14, a). Along Sumatra part of the upwelling Kelvin waves dissipate as coastal Kelvin waves of the same polarity, towards the south and north. These waves are transmitted along the Bay of Bengal coast and upwelling Rossby waves are reflected westward into the Bay of Bengal. This explains the dipole effects in the Bay of Bengal, as these waves cause thermocline and oxycline upwelling. Also, the Jet anomaly also causes the formation of coastal downwelling kelvin waves along the coasts of Sri Lanka, which propagates along the Arabian sea coast. Downwelling rossby waves are reflected westward into the Arabian Sea and may explain the results observed in this area. During negative phases (Fig 14, b), the polarity of all these waves is reversed and thus explains the opposite effect of negative phases on the oxygen .

Impact on ecosystems of changes in oxygen concentrations by IOD phases

In the Arabian Sea, during the negative phases, there is a doubling of the frequency of observation of hypoxic waters ($60 \mu\text{mol.L}^{-1}$) in the first 50 metres. In the Arabian Sea, during the negative phases, there is a doubling of the frequency of observation of hypoxic waters (60 umol) in the first

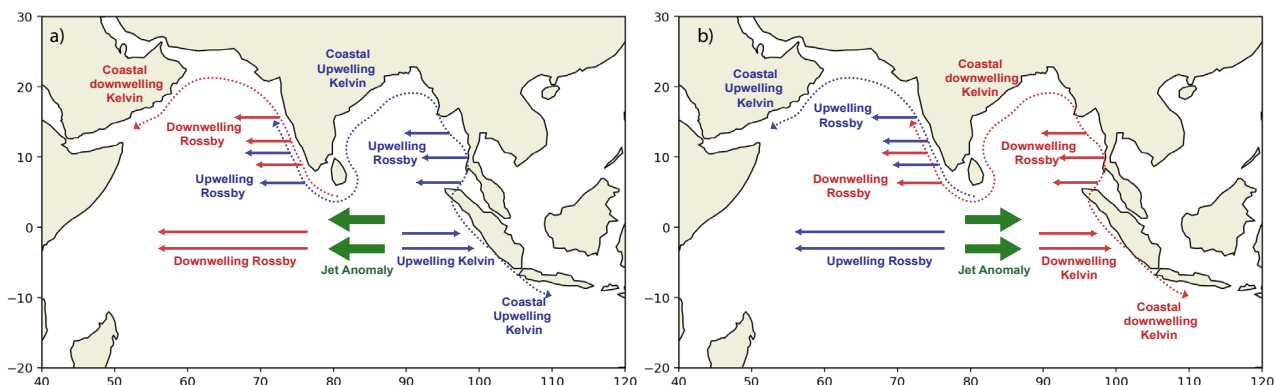


Figure 14 – Theoretical propagation pattern of the waves generated by jet anomalies during the positive (a) and negative (b) phases of the IOD.

50 metres. In the Bay of Bengal, the mean concentration of O_2 in the waters is hypoxic during the neutral phases and therefore not favourable for harbouring fish populations, especially at depth (100-200m). The positive phases decrease the O_2 concentration, aggravating the situation with a doubling, even tripling of the suboxic waters. While negative phases tend to increase the concentration of O_2 in the water column, making it favourable for sheltering pelagic populations in deeper waters. The extinction of ecosystems is not involved because the distribution of O_2 is heterogeneous in the water columns studied, but on the other hand the inaccessibility of deep waters, with low oxygen content, compresses ecological niches and can expose ecosystems to overexploitation and fragility.

Prevention of anoxic event risks

Extreme events generating anoxic surface waters occur mainly in coastal waters on the continental shelf. The waters studied in this work have O_2 concentrations approaching hypoxic concentrations, at which most macro-organisms die. Our results provide information on the risks associated with the disappearance of pelagic species for fishing. But to prevent coastal anoxia risks, more profiles measured on the continental shelf are needed. The effects of the waves propagated by the IOD are presumably the same, but it is not yet possible to quantify them.

Future work needed to improve modelling

Further work is needed to understand the complex dynamics of coastal oxygen in the northern Indian Ocean. The poor representation of oxygen dynamics in the northern Indian Ocean by models may be due to a lack of information on the effects of different processes. Other than wave propagation related to IOD, one can also add the quantification of the effect of agricultural inputs, brought by rivers, on phytoplankton populations. Also, the effect of retention of oxygen-poor water by mesoscale processes such as eddies, which are not resolved by coupled climate models, can be quantified. Research needs to be carried out on these processes in order to constrain oxygen efficiently in models.

Location of fishery resources

During negative IOD phases, tunas are generally observed more in the eastern Indian Ocean and western Arabian Sea, while during negative phases fewer tunas are caught in these areas (Lan et al. 2013). This can be explained by an upwelling of the thermocline and oxycline to the west of the basin during negative events, thus the space occupied by the tunas is concentrated more at the surface and increases their vulnerability to fishing. However, another hypothesis is studied, during negative anomalies, deep waters rich in nutrients rise to the surface and generate an increase in net primary production, thus an increase in the food resources available for the tunas, which may be the reason for their increase during negative phases and vice versa during positive phases.

5 Conclusion

By gathering several large databases, over a large time interval, This study provides a quantification of the thermocline variations according to the different phases of the IOD with a resolution of 1° , which were until now only estimated by models. Also, due to the strong coupling between the thermocline and the oxycline in the basin. It also gives an order of magnitude of the oxycline variations generated by these phases to the entire basin. These variations are one average half as large as those of the thermocline. Then, this study revealed that the different phases of the IOD have inverse effects on the frequency of observation of extreme hypoxic events. The positive phases limit these events along the west coast of India, while they encourage them in the eastern Bay of Bengal. Negative phases have the opposite effect. These results complement a lack of quantification of processes that will need to be evaluated in models. They also provide information for anticipating the evolution of ecosystems and fisheries resources, as well as evaluating the risks of extreme events. However, they need to be supplemented by work related to the dynamics of ecological niches, in particular the interannual variability of primary production.

6 Acknowledgements

I would like to sincerely thank Laure Resplandy for having received me in her research team and for having regularly supported me in my work despite the particular conditions of this internship. I also wanted to thank the geosciences department of Princeton and the ENS for the financial support provided, without which this internship would have been difficult to carry out.

References

- S. S. Acharya and M. K. Panigrahi. Eastward shift and maintenance of arabian sea oxygen minimum zone: Understanding the paradox. *Deep Sea Research Part I: Oceanographic Research Papers*, 115: 240–252, 2016.
- A. H. Altieri, S. B. Harrison, J. Seemann, R. Collin, R. J. Diaz, and N. Knowlton. Tropical dead zones and mass mortalities on coral reefs. *Proceedings of the National Academy of Sciences*, 114(14):3660–3665, 2017.
- D. Breitburg, L. A. Levin, A. Oschlies, M. Grégoire, F. P. Chavez, D. J. Conley, V. Garçon, D. Gilbert, D. Gutiérrez, K. Isensee, et al. Declining oxygen in the global ocean and coastal waters. *Science*, 359 (6371), 2018.
- P. Cayré and F. Marsac. Modelling the yellowfin tuna (*thunnus albacares*) vertical distribution using sonic tagging results and local environmental parameters. *Aquatic Living Resources*, 6(1):1–14, 1993.
- T. Dalsgaard, F. J. Stewart, B. Thamdrup, L. De Brabandere, N. P. Revsbech, O. Ulloa, D. E. Canfield, and E. F. DeLong. Oxygen at nanomolar levels reversibly suppresses process rates and gene expression in anammox and denitrification in the oxygen minimum zone off northern chile. *MBio*, 5(6), 2014.
- R. J. Diaz and R. Rosenberg. Spreading dead zones and consequences for marine ecosystems. *science*, 321 (5891):926–929, 2008.
- W. Ekau, H. Auel, H.-O. Pörtner, and D. Gilbert. Impacts of hypoxia on the structure and processes in pelagic communities (zooplankton, macro-invertebrates and fish). *Biogeosciences*, 7(5):1669–1699, 2010.
- W. Fu, F. Primeau, J. Keith Moore, K. Lindsay, and J. T. Randerson. Reversal of increasing tropical ocean hypoxia trends with sustained climate warming. *Global Biogeochemical Cycles*, 32(4):551–564, 2018.
- K. P. Helm, N. L. Bindoff, and J. A. Church. Observed decreases in oxygen content of the global ocean. *Geophysical Research Letters*, 38(23), 2011.
- M. C. Ingham, S. K. Cook, and K. Hausknecht. Oxycline characteristics and skipjack tuna distribution in the southeastern tropical atlantic. *Fish. Bull.*, 75: 857–865, 1977.
- T. Ito, S. Minobe, M. C. Long, and C. Deutsch. Upper ocean o₂ trends: 1958–2015. *Geophysical Research Letters*, 44(9):4214–4223, 2017.
- S. Jana, A. Gangopadhyay, and A. Chakraborty. Impact of seasonal river input on the bay of bengal simulation. *Continental Shelf Research*, 104:45–62, 2015.
- R. F. Keeling, A. Körtzinger, and N. Gruber. Ocean deoxygenation in a warming world. 2009.
- K.-W. Lan, K. Evans, and M.-A. Lee. Effects of climate variability on the distribution and fishing conditions of yellowfin tuna (*thunnus albacares*) in the western indian ocean. *Climatic change*, 119(1):63–77, 2013.
- L. A. Levin. Manifestation, drivers, and emergence of open ocean deoxygenation. *Annual Review of Marine Science*, 10(1):229–260, 2018.
- S. Levitus, R. A. Locarnini, T. P. Boyer, A. V. Mishonov, J. I. Antonov, H. E. Garcia, O. K. Baranova, M. M. Zweng, D. R. Johnson, and D. Seidov. World ocean atlas 2009. 2010.
- M. C. Long, C. Deutsch, and T. Ito. Finding forced trends in oceanic oxygen. *Global Biogeochemical Cycles*, 30(2):381–397, 2016.
- S. W. A. Naqvi, H. Naik, D. Jayakumar, M. Shailaja, and P. Narvekar. Seasonal oxygen deficiency over the western continental shelf of india. In *Past and present water column anoxia*, pages 195–224. Springer, 2006.
- S. W. A. Naqvi, H. Naik, A. Jayakumar, A. K. Pratihary, G. Narvenkar, S. Kurian, R. Agnihotri, M. Shailaja,

- and P. V. Narvekar. Seasonal anoxia over the western indian continental shelf. *Indian Ocean biogeochemical processes and ecological variability*, 185: 333–345, 2009.
- A. Oschlies, P. Brandt, L. Stramma, and S. Schmidtko. Drivers and mechanisms of ocean deoxygenation. *Nature Geoscience*, 11(7):467–473, 2018.
- V. Parvathi, I. Suresh, M. Lengaigne, C. Ethé, J. Vialard, M. Levy, S. Neetu, O. Aumont, L. Resplandy, H. Naik, et al. Positive indian ocean dipole events prevent anoxia off the west coast of india. 2017.
- L. Resplandy, M. Lévy, L. Bopp, V. Echevin, S. Pous, V. Sarma, and D. Kumar. Controlling factors of the oxygen balance in the arabian sea's omz. 2012.
- N. Saji, B. Goswami, P. Vinayachandran, and T. Yamagata. A dipole mode in the tropical indian ocean. *Nature*, 401(6751):360–363, 1999.
- S. Schmidtko, L. Stramma, and M. Visbeck. Decline in global oceanic oxygen content during the past five decades. *Nature*, 542(7641):335–339, 2017.
- F. A. Schott and J. P. McCreary Jr. The monsoon circulation of the indian ocean. *Progress in Oceanography*, 51(1):1–123, 2001.
- F. A. Schott, S.-P. Xie, and J. P. McCreary Jr. Indian ocean circulation and climate variability. *Reviews of Geophysics*, 47(1), 2009.
- I. M. Sokolova. Energy-limited tolerance to stress as a conceptual framework to integrate the effects of multiple stressors. *Integrative and comparative biology*, 53(4):597–608, 2013.
- T. F. Stocker, D. Qin, G.-K. Plattner, M. Tignor, S. K. Allen, J. Boschung, A. Nauels, Y. Xia, V. Bex, P. M. Midgley, et al. Climate change 2013: The physical science basis. *Contribution of working group I to the fifth assessment report of the intergovernmental panel on climate change*, 1535, 2013.
- L. Stramma, G. C. Johnson, J. Sprintall, and V. Mohrholz. Expanding oxygen-minimum zones in the tropical oceans. *science*, 320(5876):655–658, 2008.
- L. Stramma, E. D. Prince, S. Schmidtko, J. Luo, J. P. Hoolihan, M. Visbeck, D. W. Wallace, P. Brandt, and A. Kötzinger. Expansion of oxygen minimum zones may reduce available habitat for tropical pelagic fishes. *Nature Climate Change*, 2(1):33–37, 2012.
- I. Suresh, J. Vialard, M. Lengaigne, T. Izumo, V. Parvathi, and P. Muraleedharan. Sea level interannual variability along the west coast of india. *Geophysical Research Letters*, 45(22):12–440, 2018.
- B. Thamdrup. New pathways and processes in the global nitrogen cycle. *Annual Review of Ecology, Evolution, and Systematics*, 43:407–428, 2012.
- R. Vaquer-Sunyer and C. M. Duarte. Thresholds of hypoxia for marine biodiversity. *Proceedings of the National Academy of Sciences*, 105(40):15452–15457, 2008.
- D. Yuan and H. Liu. Long-wave dynamics of sea level variations during indian ocean dipole events. *Journal of physical oceanography*, 39(5):1115–1132, 2009.